OH$^+$ in Diffuse Molecular Clouds

A.J. Porras[1,2], S.R. Federman[1], D.E. Welty[3], and A.M. Ritchey[4]

ABSTRACT

Near ultraviolet observations of OH$^+$ and OH in diffuse molecular clouds reveal a preference for different environments. The dominant absorption feature in OH$^+$ arises from a main component seen in CH$^+$ (that with the highest CH$^+$/CH column density ratio), while OH follows CN absorption. This distinction provides new constraints on OH chemistry in these clouds. Since CH$^+$ detections favor low-density gas with small fractions of molecular hydrogen, this must be true for OH$^+$ as well, confirming OH$^+$ and H$_2$O$^+$ observations with the *Herschel* Space Telescope. Our observed correspondence indicates that the cosmic ray ionization rate derived from these measurements pertains to mainly atomic gas. The association of OH absorption with gas rich in CN is attributed to the need for high enough density and molecular fraction before detectable amounts are seen. Thus, while OH$^+$ leads to OH production, chemical arguments suggest that their abundances are controlled by different sets of conditions and that they coexist with different sets of observed species. Of particular note is that non-thermal chemistry appears to play a limited role in the synthesis of OH in diffuse molecular clouds.

Subject headings: ISM: lines and bands – ISM: molecules – ultraviolet: ISM – astrochemistry

1. Introduction

The chemistry of diffuse molecular clouds is mainly driven by ion-molecule reactions (e.g., van Dishoeck & Black 1986; Le Petit et al. 2004). Many of the intermediate species

[1]Department of Physics and Astronomy, University of Toledo, Toledo, OH 43606; steven.federman@utoledo.edu

[2]Department of Physics and Astronomy, University of North Carolina, Chapel Hill, NC 27599; aporras@live.unc.edu

[3]Department of Astronomy & Astrophysics, University of Chicago, 5640 S. Ellis Ave., Chicago, IL 60637; dwelty@oddjob.uchicago.edu

[4]Department of Astronomy, University of Washington, Seattle, WA 98195; aritchey@astro.washington.edu

are ions, and because they rapidly react with neutrals (especially H_2 or abundant atoms) and electrons, their abundances tend to be low. A major pathway to OH involves the intermediates OH^+, H_2O^+, and H_3O^+ (e.g., Federman et al. 1996 and references therein). These oxygen-bearing ions are especially important; they provide a means to infer the cosmic ray ionization rate in diffuse molecular gas. This arises because cosmic rays ionize atomic and molecular hydrogen, leading to H^+ and H_3^+. The hydrogen ions transfer their charge to O, producing first O^+ and then the molecular ions OH_n^+ through ion-molecule reactions.

New, sensitive observations are now able to detect such intermediate species. Wyrowski et al. (2010) observed the sub-mm ground-state transitions of OH^+ in absorption from diffuse molecular clouds toward Sgr B2(M) with the Atacama Pathfinder Experiment. Sub-mm measurements with the *Herschel* Space Telescope revealed absorption from OH^+, H_2O^+, and H_3O^+ from diffuse molecular clouds toward distant star-forming regions (Neufeld et al. 2010; Gerin et al. 2010; Ossenkopf et al. 2010). Neufeld et al. showed that the observed OH^+/H_2O^+ ratio indicates that absorption from these molecules arises from material with small H_2 fractions. The OH^+ abundance relative to H provided an estimate of the cosmic ray ionization rate, consistent with earlier determinations. Absorption from OH^+ was also detected at near ultraviolet wavelengths through measurements acquired with the VLT/UVES instrument (Krełowski et al. 2010). Krełowski et al. suggested that OH^+ absorption traces CH^+ the best among the molecular species seen at optical wavelengths.

We build on these earlier observations through a detailed analysis of OH^+ and OH absorption in the near ultraviolet. While line-of-sight results are emphasized in earlier ground-based work, the focus here is on directions showing component structure with varying molecular abundances. We discuss results for VLT/UVES observations of BD$-14°5037$, HD149404, HD154368, and HD183143 because they reveal the clearest separation between strong CH^+ and CN absorption. Our previous work (e.g., Pan et al. 2005) showed that CH^+ absorption favors low density, molecule poor gas, while CN is associated with denser, molecule rich material. This separation allows us to study the chemistry of oxygen-bearing species in diffuse molecular clouds in greater detail than was possible before.

2. Observations

Data below 4000 Å, acquired with the Ultraviolet and Visual Echelle Spectrograph (UVES) of the Very Large Telescope (VLT) at Cerro Paranal, Chile, were obtained from the European Southern Observatory Science Archive Facility. Spectra of all four stars were acquired under program 065.I-0526 (PI: E. Roueff); additional data for HD149404 and HD154368 were obtained under program 082.C-0566 (PI: Y. Beletsky). Both observing

programs utilized the central wavelength setting at 3460 Å and a 0.4 arcsec slit. The UVES pipeline reduction software was applied to the data in optimal extraction mode to produce merged spectra providing continuous coverage from 3050 to 3870 Å. Finally, for each observing program, the individual exposures of a given target were coadded to produce a single high S/N spectrum. For HD149404 and HD154368, the spectral resolution is 3.8 km s^{-1} ($R = 79,000$), since the observations employed CCD binning of 1×1. For BD$-14°5037$ and HD183143, where 1×2 binning was used, the resolution is 4.2 km s^{-1} ($R = 71,000$).

Spectra of K I λ7699 were also used in the analysis. They came from archival UVES data (BD$-14°5037$), Kitt Peak National Observatory Coude Feed data for HD149404 and HD154368 (Welty, unpublished), and McDonald Observatory 2.7 m coude observations for HD183143 (McCall et al. 2002).

Systematic fluctuations, with scale and amplitude similar to some of the true interstellar features and at very similar (geocentric) velocities, were noted near the wavelengths expected for the OH$^+$ line in the extracted spectra of several sight lines. This apparent residual detector pattern is present even in the spectra of some stars with very weak absorption from other molecular species, where the OH$^+$ line would not be expected to be detectable. The normalized spectra of those stars (HD116658, HD212571, HD182985) were used as templates to remove the residual detector pattern. Division by the template spectra generally yielded smoother continua and reduced noise near the OH$^+$ line.

The divided spectra were shifted to heliocentric velocities, combined (for sight lines observed under both programs), and normalized via low-order polynomial fits to the continuum regions. For the four stars considered here, the S/N ratios measured in the continuum fits range from about 100–210 (per resolution element) near the OH lines ($\lambda\lambda$3078, 3080) to about 390–700 near the OH$^+$ line λ3584. The resulting spectra, along with relatively weak lines of CH, CH$^+$, and CN, are shown in Figures 1 through 4. When CN λ3579 was especially weak, the stronger line, λ3874, is displayed.

Total equivalent widths and column densities were obtained from the combined, normalized spectra by integrating the residual intensity and apparent optical depth (AOD), respectively, over the profiles of detected absorption lines. The 1σ uncertainties on the equivalent widths include contributions from photon noise and continuum fitting, which are generally of comparable magnitude for relatively weak, narrow, unresolved lines. Column densities and velocities for "individual" components discernible in the profiles of various atomic and molecular species were determined via independent multi-component fits to the profiles (e.g., Welty, Hobbs, & Morton 2003). Table 1 summarizes the results for the molecular species; further details about the analysis on CH, CH$^+$, and CN will appear in Welty et al. (2013, in preparation, hereafter Welty2013). For the weak OH and OH$^+$ lines, the total

column densities obtained from the profile fits are consistent with the AOD estimates.

For the most part, the molecular data adopted in our analyses are the same as those used in previous studies (e.g., Federman et al. 1996; Felenbok & Roueff 1996; Weselak et al. 2009a,b; Krełowski et al. 2012). However, the wavelength for CH $\lambda 3143$ and the OH^+ f-value are taken from more recent work. The use of the wavelengths quoted by Lien (1984) for the CH $C - X$ band yielded components that were shifted by about 2 km s^{-1} relative to other lines of CH. This discrepancy was removed when the data of Bembenek et al. (1997) were adopted. As for the OH^+ f-value, the value quoted by de Almeida & Singh (1981) and used by Krełowski et al. (2010) is no longer the preferred one. The measurements of Brzozowski et al. (1974), which were utilized by de Almeida & Singh (1981), were affected by space charge, resulting in shortened lifetimes. These effects were analyzed by Curtis & Erman (1977), who determined a corrected lifetime of 2.4±0.3 μs; subsequent measurements by Möhlmann et al. (1978) based on an independent technique and theoretical calculations by Merchán et al. (1991) yielded comparable lifetimes. The recommended f-value for future studies is 1.14×10^{-3}, nearly a factor of 3 smaller than that considered in earlier studies.

3. Results and Discussion

Our total equivalent widths for CH, CH^+, CN, OH^+, and OH lines in the near ultraviolet are consistent with those of Weselak et al. (2009a, b) and Krełowski et al. (2010, 2012). We note, however, that their values are often somewhat larger than ours, due perhaps to the additional data incorporated here and/or to slight differences in continuum placement. The comparison is discussed in more detail in our larger survey of optical molecular absorption seen in UVES spectra (Welty2013).

Table 1 compiles the component structure for the four sight lines. The column densities for CH, CH^+, and CN are based on all available data (Welty2013). The OH features are associated with the strongest CN components. Absorption from OH^+, on the other hand, favors strong CH^+ components and especially those with the highest $N(CH^+)/N(CH)$ ratio; these components tend to lack CN lines. Krełowski et al. (2010) suggested that OH^+ is associated with CH^+, but their work focused on OH^+ detections. Figures 1 to 4 illustrate the correspondences involving the strongest components in OH^+ and OH. Some possible weak OH^+ components (at $\leq 3\sigma$) may be related to weak components seen in strong lines of CH, CH^+, Na I D, and/or K I at longer wavelengths, which is representative of material dominated by atomic hydrogen. The likelihood of these being detections is discussed below.

As discussed in our previous work (e.g., Pan et al. 2005), different species have their

largest abundances in specific regions within individual diffuse clouds. Because CH^+ is destroyed by reactions with both atomic and molecular hydrogen, as well as electrons, it is generally found in low density gas with small H_2 fractions. Significant abundances of precursor molecules are required for observable amounts of CN, so that CN probes denser regions with larger H_2 fractions. The CH radical is found in both types of gas, but larger column densities are usually seen in material traced by CN.

The same seems to apply to OH^+ and OH. The connection between OH^+ and CH^+ (and possibly neutral atoms) indicates that OH^+ detections also favor low density gas. Thus, our optical results are consistent with the conclusions of Neufeld et al. (2010) from analysis of sub-mm data acquired with *Herschel*. In particular, absorption from OH^+ and H_2O^+ in diffuse molecular clouds occurs at velocities most similar to those seen in 21 cm absorption. The inferred OH^+/H_2O^+ abundance ratios imply H_2 fractions less than about 10%. On the other hand, the association of OH with CN-rich gas reveals that OH is found in gas with higher densities, in excess of about 100 cm^{-3} (e.g., Pan et al. 2005).

That difference in behavior is consistent with simple chemical arguments. The intermediate species (OH^+) is rapidly destroyed by reactions with H_2, like the situation for CH^+. The production of OH from OH^+ requires additional steps: reactions involving H_2 lead first to H_2O^+ and then H_3O^+, followed by dissociative recombination (H_nO^+ + e). Denser gas also usually has greater amounts of extinction, which diminishes the effects of OH photodissociation. This pictures runs counter to models that produce OH in gas heated by turbulent dissipation (e.g., Godard et al. 2009), heated by transient microstructure (Cecchi-Pestellini et al. 2009), or affected by the injection of hot H_2 (e.g., Cecchi-Pestellini et al. 2012) because OH is associated with CH^+ in these models. Furthermore, a clearer picture emerges for the similarity in component structures seen in CN and CO spectra for directions with $N(CO) \geq$ few $\times 10^{14}$ cm^{-2} (e.g., Pan et al. 2005; Sonnentrucker et al. 2007; Sheffer et al. 2008). In such diffuse molecular clouds, CO arises from a series of reactions initiated by C^+ + OH $\rightarrow$ CO^+ + H, followed by production of HCO^+ and then CO through dissociative recombination. Thus, while OH^+ occasionally is seen in denser components, it is efficiently consumed there in the chain leading to OH and CO.

Instead, most of the production of OH, as well as all of the OH^+, therefore appears to be tied to cosmic ray ionization. That behavior allows us to estimate the cosmic ray ionization rate in the components shown in Table 1. Our analysis is based on the rate equations in Appendix of Federman et al. (1996). While these expressions do not incorporate the effects of PAH species on ionization, Hollenbach et al. (2012) included these effects in their modeling, allowing us to estimate the changes that would occur. We rely on rates and rate coefficients given in Federman et al. for the most part, but update the dissociative

recombination coefficients and branching fractions when necessary from the compilation of Florescu-Mitchell & Mitchell (2006). The theoretical study of charge exchange between H^+ and O by Stancil et al. (1999) produces a rate coefficient very similar to the one used by us previously when a temperature of 80 K is considered. A gas density of 100 cm^{-3} is adopted here. The complete list of inputs can be found in Welty2013.

The starting point is the steady-state rate equation for OH^+ in terms of fractional abundances, $x(X)$ given by

$$x(OH^+) = \frac{k_3 x(H_2)}{k_4 x(H_2)} \frac{k_1 x(O)}{k_2 x(H) + k_3 x(H_2)} \frac{5\zeta_p x(H)}{2\alpha(He^+)x_e n + k_1 x(O)n}, \tag{1}$$

where k_i are rate coefficents, ζ_p is the primary cosmic ray ionization rate (equal to 0.5 ζ_{H_2} given in Indriolo & McCall 2012), $\alpha(He^+)$ is the rate coefficient for He^+ recombination, x_e is the ionization fraction, and n is the gas density $[n(H) + 2\,n(H_2)]$. For the gas rich in OH^+, we adopt $x(H) = 10x(H_2)$. The ionization fraction is taken to be 2×10^{-4}, so that it is slightly larger than only counting electrons from carbon ionization. Solving for ζ_p with the rate coefficients noted above yields $\zeta_p \approx 1.3 \times 10^{-8}\,N(OH^+)/N(H)$, where $N(H)$ equals $N(H\ I) + 2N(H_2)$. For comparison, Hollenbach et al. (2012) provide a similar expression with a factor of 4.3×10^{-8} for our adopted temperature and density.

The final step is the determination of $N(H)$. For HD149404 and HD154368, values are available from Diplas & Savage (1994) and Rachford et al. (2002). For the other directions, we estimated $N(H)$ from the total K I column density, using the relationship in Welty & Hobbs (2001). We are confident in these estimates because the relationship gives values for $N(H)$ toward HD149404 and HD154368 within about 10% of the measured values. Finally, we estimate $N(H)$ for each component by determining its fraction of the total $N(K\ I)$ multiplied by the total $N(H)$. While this step is less secure, the relationship in Welty & Hobbs spans the range for most of the values considered here.

For OH, we consider $x(H) = x(H_2)$, $T = 50$ K, and $n = 300$ cm^{-3}, because its absorption appears to be associated with denser gas. Then eqns. (A2) and (A3) in Federman et al. (1996) are reduced to a simpler form for $x(OH)$,

$$x(OH) = x(OH^+)\frac{k_4 x(H_2)}{k_6 x(C^+)} \frac{\beta'(H_3O^+)}{\beta(H_3O^+)}. \tag{2}$$

Here $\beta(X)$ is the dissociative recombination rate coefficient for molecular ion X, with a prime denoting the branch leading to OH. In other words, once OH^+ is formed, OH arises directly from the sequence, OH^+ to H_2O^+ to H_3O^+ to OH without any branches for the

adopted conditions. OH destruction by reactions with C^+ is also more important than photodissociation for the sight lines studied here because the optical depth at ultraviolet wavelengths due to grains, $\tau_{uv} \geq 2$. Combining our eqns. (1) and (2) and our set of input parameters leads to $\zeta_p \approx 8.4 \times 10^{-10} \, N(OH)/N(H)$.

For most of the components shown in Table 1, our estimate for ζ_p ranges from 0.2 to 2.0×10^{-16} s^{-1} (see last two columns), consistent with other recent determinations. For the one component with both OH^+ and OH, that toward BD$-14°5037$ at about 5 km s^{-1}, the estimate from OH^+ is 0.5×10^{-16} s^{-1}, while that from OH is 0.3×10^{-16} s^{-1}. They can be made to agree with slightly different values for n (suggesting that the conditions vary along the line of sight because different conditions were adopted for the two estimates). For that matter, all the estimates for a given sight line could be make consistent by slight changes of order a factor of a few in n. Such relatively small changes are not unreasonable in light of earlier analyses of similar material. Zsargó & Federman (2003) inferred densities of about 10 to a few hundred cm^{-3} from neutral carbon excitation for directions with chemical conditions like those seen here for the OH^+ components. Similarly, densities between about 100 and 1000 cm^{-3} seem appropriate for gas rich in CN (e.g., Sheffer et al. 2008). For instance, C_2 excitation for these clouds typically yields densities of 200 to 400 cm^{-3} (e.g., Sonnentrucker et al. 2007). Thus, these diffuse molecular clouds have primary cosmic ray ionization rates of about 1×10^{-16} s^{-1}. The exceptions to these results are the components only tentatively detected in OH^+ (and atomic species). They suggest ionization rates greater than about 5×10^{-16} s^{-1} and are deemed suspect.

We can compare our estimates for ζ_p with others. From analyses of H_3^+ absorption, Indriolo & McCall (2012) found values ranging from ≤ 0.2 to about 5×10^{-16} s^{-1}, with the detections having uncertainties of 50%. In particular, Indriolo & McCall obtained (in units of 10^{-16} s^{-1}) ≤ 0.2 (BD$-14°5037$), ≤ 1.3 (HD149404), 2.10 ± 1.31 (HD154368), and 5.30 ± 4.12 and 3.91 ± 2.96 for the -10 and $+5$ km s^{-1} components toward HD183143. The general agreement is encouraging and could be made better by using the same set of physical conditions. Hollenbach et al. (2012) provide an analytic expression for the OH^+ abundance in diffuse molecular clouds that includes PAH species in the ionization balance. For T of 80 K, their relationship for ζ_p is $4.3 \times 10^{-8} \, N(OH^+)/N(H)$, with a proportionality constant about 3 times larger than ours. This more comprehensive treatment suggests the need for us to start with densities more like 30 cm^{-3} for the material with detectable amounts of OH^+ (and CH^+).

Fig. 3 in Hollenbach et al. shows chemical results for conditions appropriate for the clouds studied here. The OH abundance peaks at larger extinctions into a cloud, much like we infer. The peak OH abundance relative to that for OH^+ is about 10, similar to our

results for the +5 km s^{-1} component toward BD$-14°5037$. The results in Table 1 reveal a large range in $N(OH)/N(OH^+)$, however, from less than 3 to greater than 60. More detailed comparisons require modeled column densities.

Indriolo et al. (2012) compared estimates for the cosmic ray ionization rate in diffuse clouds toward W51 from sub-mm observations of OH^+ and H_2O^+ with H_3^+ measurements in nearby sight lines. The analysis is based on the premise that OH^+ and H_2O^+ probe predominantly atomic gas, while H_3^+ is associated with H_2. To bring the estimates into agreement, they deduced an efficiency factor for producing OH^+ from ionization of H atoms of about 0.10. The comparisons between our results and those of Indriolo & McCall (2012) do not require a low efficiency factor. More precise data and detailed modeling are needed to clarify the situation.

4. Conclusions

VLT/UVES measurements reveal that absorption from OH^+ and OH arise from different environments. Gas with lower densities and smaller H_2 fractions provide the conditions for observable amounts of OH^+; this material is also rich in CH^+. Our results at near ultraviolet wavelengths confirm the conclusions reached by studying sub-mm absorption (e.g., Neufeld et al. 2010). The OH components, on the other hand, are associated with CN-rich gas with higher densities and larger H_2 fractions.

Since OH absorption is generally not seen in the strongest CH^+ components, the chemical routes for the two molecules must differ. We suggest that cosmic ray ionization is the dominant source for OH in diffuse molecular clouds. Simple chemical arguments are used to infer the cosmic ray ionization rate, finding values of $\approx 1 \times 10^{-16}$ s^{-1}. For the one component with both OH^+ and OH absorption in our sample, the analysis indicates that the conditions along the line of sight may vary somewhat, with temperatures varying about a factor 2 and densities about a factor of 3. Such variation is not unreasonable, as it is seen in more comprehensive modeling efforts (e.g., van Dishoeck & Black 1986). Our estimates are also consistent with those inferred from H_3^+ observations (e.g., Indriolo & McCall 2012) and from chemical models including the effects of PAH molecules (Hollenbach et al. 2012). The differences can easily be accommodated with small changes in gas density. These findings will be incorporated into our survey (Welty2013) of a large number of directions to discern the range of densities and cosmic ray ionization rates for diffuse molecular clouds.

REFERENCES

Bembenek, Z., Kępa, R., & Rytel, M. 1997, J. Molec. Spectrosc., 183, 1

Brzozowski, J., Elander, N., Erman, P., & Lyyra, M. 1974, ApJ, 193, 741

Cecchi-Pestellini, C., Duley, W.W., & Williams, D.A. 2012, ApJ, 755, 119

Cecchi-Pestellini, C., Williams, D.A., Viti, S., & Casu, S. 2009, ApJ, 706, 1429

Curtis, L.J., & Erman, P. 1977, J. Opt. Soc. Amer., 67, 1218

de Almeida, A.A., & Singh, P.D. 1981, A&A, 95, 383

Diplas, A., & Savage, B.D. 1994, ApJS, 93, 211

Federman, S.R., Weber, J., & Lambert, D.L. 1996, ApJ, 463, 181

Felenbok, P., & Roueff, E. ApJ, 465, L57

Florescu-Mitchell, A.I., & Mitchell, J.B.A. 2006, Phys. Rep., 430, 277

Gerin, M., De Luca, M., Black, J., et al. 2010, A&A, 518, L110

Godard, B., Falgarone, E., & Pineau des Forêts, G. 2009, A&A, 495, 847

Hollenbach, D., Kaufman, M.J., Neufeld, D., Wolfire, M., & Goicoechea, J.R. 2012, ApJ, 754, 105

Indriolo, N., & McCall, B.J. 2012, ApJ, 745, 91

Indriolo, N., Neufeld, D.A., Gerin, M. et al. 2012, ApJ, 758, 83

Krełowski, J., Beletsky, Y., & Galazutdinov, G.A. 2010, ApJ, 719, L20

Krełowski, J., Galazutdinov, G., & Gnaciński, P. 2012, Astron. Nachr., 333, 627

Le Petit, F., Roueff, E., & Herbst, E. 2004, A&A, 417, 993

Lien, D.J. 1984, ApJ, 284, 578

McCall, B.J., Hinkle, K.H., Geballe, T.R. et al. 2002, ApJ, 567, 391

Merchán, M., Malmqvist, P.-Å, & Roos, B.O. 1991, Theor. Chim. Acta, 79, 81

Möhlmann, G.R., Bhutani, K.K., de Heer, F.J., & Tsurubuchi, S. 1978, Chem. Phys., 31, 273

Neufeld, D.A., Goicoechea, J.R., Sonnentrucker, P., et al. 2010, A&A, 521, L10

Ossenkopf, V., Müller, H.S.P., Lis, D.C., et al. 2010, A&A, 518, L111

Pan, K., Federman, S.R., Sheffer, Y., & Andersson, B-G 2005, ApJ, 663, 986

Rachford, B.L., Snow, T.P., Tumlinson, J. et al. 2002, ApJ, 577, 221

Sheffer, Y., Rogers, M., Federman, S.R., et al. 2008, ApJ, 687, 1075

Sonnentrucker, P., Welty, D.E., Thorburn, J.A., & York, D.G. 2007, ApJS, 168, 58

Stancil, P.C., Schultz, D.R., Kimura, M., et al. 1999, A&A, 140, 225

van Dishoeck, E.F., & Black, J.H. 1986, ApJS, 62, 109

Welty, D.E., & Hobbs, L.M. 2001, ApJS, 133, 345

Welty, D.E., Hobbs, L.M., & Morton, D.C. 2003, ApJS, 147, 61

Weselak, T., Galazutdinov, G., Beletsky, Y., & Krełowski, J. 2009b, A&A, 499, 783

Weselak, T., Galazutdinov, G.A., Musaev, F.A., Beletsky, Y., & Krełowski, J. 2009a, A&A, 495, 189

Wyrowski, F., Menten, K.M., Güsten, R., & Belloche, A. 2010, A&A, 518, A26

Zsargó, J., & Federman, S.R. 2003, ApJ, 589, 319

Table 1. Component Structures

Star	CH			CH$^+$			CN			OH$^+$			OH			ζ_p	
	$N12$	b	$v_\odot$	$N12$	b	$v_\odot$	$N12$	b	$v_\odot$	$N12$	b	$v_\odot$	$N13$	b	$v_\odot$		
BD$-$14 5037	3.0	[2.0]	-13.2	3.9	[3.6]	-12.8			$\cdots$	2.7	[2.0]	-11.9	≤ 2.8		$\cdots$	1.6	$\cdots$
	36.0	1.1	-6.8	9.7	[2.5]	-7.4	19.5	[0.6]	-6.7	≤ 2.9		$\cdots$	12.4	[2.5]	-5.8	$\cdots$	0.4
			$\cdots$	18.0	[2.5]	1.0			$\cdots$			$\cdots$			$\cdots$	$\cdots$	$\cdots$
	45.0	2.5	3.3	36.2	[2.5]	5.4	6.5	[0.8]	3.2	8.9	3.5	4.7	7.8	[2.5]	4.3	0.5	0.3
	10.0	[2.5]	8.7			$\cdots$	2.1	[0.8]	9.0			$\cdots$			$\cdots$	$\cdots$	$\cdots$
HD 149404	6.2	2.0	-18.7	5.3	2.8	-16.9	0.6	[1.0]	-19.6	1.9	[2.5]	-19.2	≤ 1.7		$\cdots$	0.2	$\cdots$
			$\cdots$			$\cdots$			$\cdots$	4.0	[2.5]	-12.8	≤ 1.7		$\cdots$	5.5	$\cdots$
	6.3	2.1	-7.8	18.9	3.3	-6.7			$\cdots$	5.0	[1.0]	-7.0	≤ 1.6		$\cdots$	1.2	$\cdots$
	2.9	[1.2]	-3.5			$\cdots$			$\cdots$	3.0	[2.0]	-1.8	≤ 2.5		$\cdots$	1.3	$\cdots$
	12.4	1.1	0.6	22.0	1.9	0.0	2.9	[1.0]	-0.4	≤ 3.0		$\cdots$	4.3	2.5	1.1	$\cdots$	0.3
HD 154368	2.1	[1.0]	-20.8	0.5	[2.5]	-22.1			$\cdots$			$\cdots$			$\cdots$	$\cdots$	$\cdots$
			$\cdots$	1.1	[2.5]	-14.8			$\cdots$			$\cdots$			$\cdots$	$\cdots$	$\cdots$
			$\cdots$			$\cdots$			$\cdots$	1.7	[1.5]	-10.7	≤ 2.0		$\cdots$	3.3	$\cdots$
	9.4	[1.2]	-5.4	13.7	[2.0]	-5.6			$\cdots$	4.2	[2.0]	-5.1	≤ 2.4		$\cdots$	0.5	$\cdots$
	47.5	1.1	-2.4	7.5	[2.0]	-1.5	24.3	0.8	-2.5	≤ 2.9		$\cdots$	17.9	1.5	-2.0	$\cdots$	0.8
	2.1	[1.0]	1.3			$\cdots$			$\cdots$	1.6	[1.5]	0.5	≤ 2.6		$\cdots$	1.3	$\cdots$
			$\cdots$	0.4	[2.5]	3.5			$\cdots$			$\cdots$			$\cdots$	$\cdots$	$\cdots$
HD 183143	18.3	3.1	-9.5	31.5	2.4	-10.6	0.5	[1.0]	-10.2	11.0	1.1	-11.6	≤ 3.9		$\cdots$	1.9	$\cdots$
			$\cdots$			$\cdots$			$\cdots$	2.8	[1.5]	-4.9	≤ 4.0		$\cdots$	6.1	$\cdots$
	2.3	[1.5]	0.5	3.9	[2.0]	0.6			$\cdots$	3.1	[1.5]	1.9	≤ 5.1		$\cdots$	1.6	$\cdots$
	30.9	2.0	5.3	37.4	1.8	5.3	3.2	[1.0]	5.7	≤ 3.6		$\cdots$	7.7	[2.5]	5.6	$\cdots$	0.6

Note. — Column densities (in cm^{-2}) are multiplied by power of ten given in header; b and $v_\odot$ are in km s^{-1}. OH$^+$ and OH upper limits are based on fits with b and $v_\odot$ taken from results for detected species in the component. The cosmic ray ionization rates have units of 10^{-16} s^{-1}. Values for b in square braces were fixed in profile fits. The sum of the results for $J = 0$ and $J = 1$ are shown for the CN column density. The first (second) entry for ζ_p comes from our OH$^+$ (OH) analysis
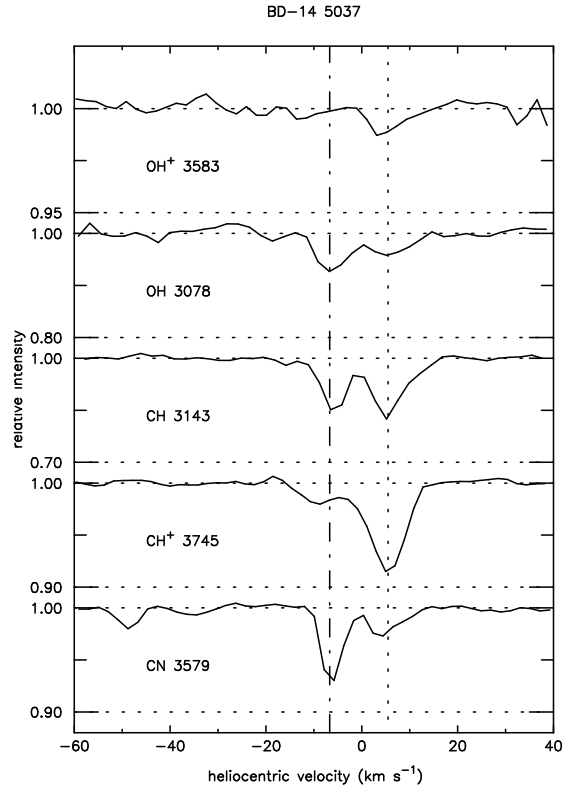
Fig. 1.— Absorption from OH$^+$, OH, CH, CH$^+$, and CN toward BD−14°5037. The wavelengths of each feature are indicated. The feature near −50 km s^{-1} is the R(1) line of CN. Note that the vertical scales differ from panel to panel. The dotted vertical line highlights the main OH$^+$/CH$^+$ component in other species. The dot-dashed line indicates the main OH/CN component.
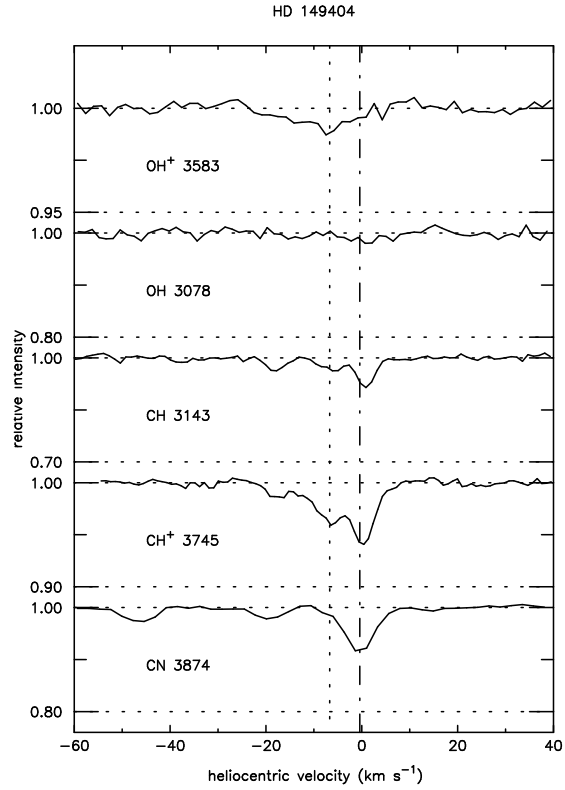
Fig. 2.— Same as Fig. 1 for absorption toward HD149404. CN $\lambda 3579$ is very weak; the stronger line at 3874 Å is shown.
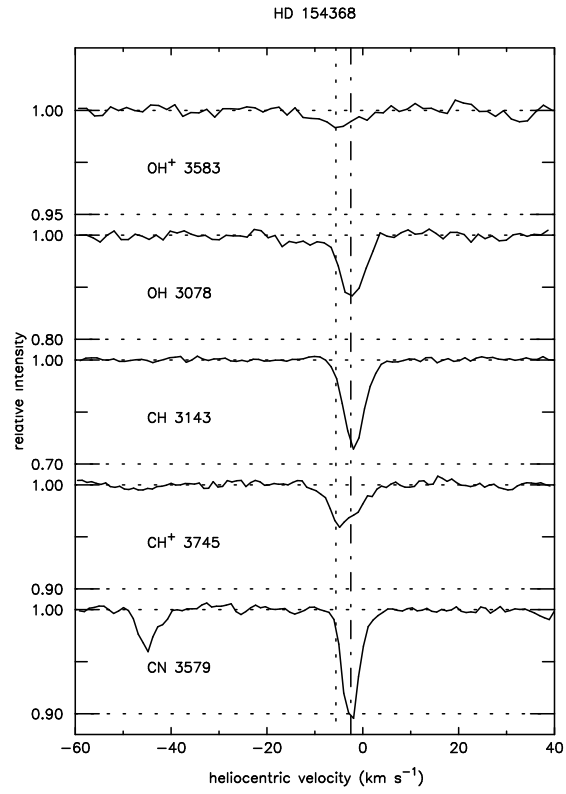
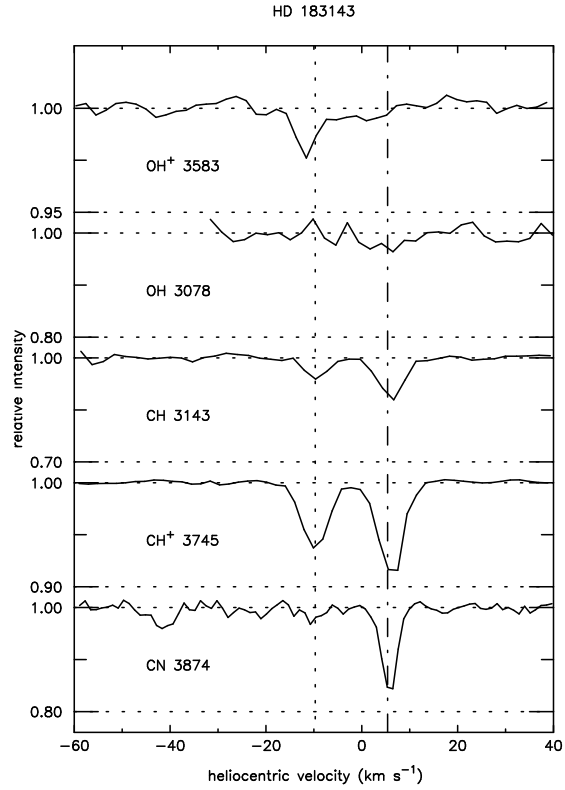Fig. 3.— Same as Fig. 1 for absorption toward HD154368.

Fig. 4.— Same as Fig. 1 for absorption toward HD183143. CN λ3579 is very weak toward this star; CN λ3874 is shown instead.